Supporting Online Material for

Synthetic Gene Networks That Count

Ari E. Friedland, Timothy K. Lu, Xiao Wang, David Shi, George Church,
James J. Collins*

*To whom correspondence should be addressed. E-mail: jcollins@bu.edu

This PDF file includes

SUPPLEMENTARY ONLINE MATERIALS

Authors' Contributions

AEF and JJC designed the RTC counters; AEF built and tested the RTC counters, with assistance from DS; XW conducted all of the modeling work; TKL, JJC and GC designed the DIC counters; TKL built and tested the DIC counters and contributed to building the RTC counters; AEF, TKL, XW, DS, GC and JJC analyzed the data and wrote the paper.

Materials and Methods

1. RTC Counter Plasmid Construction

RTC Counter plasmids were constructed using basic molecular cloning techniques (*S1*). New England Biolab's restriction endonucleases, T4 DNA Ligase, and Taq Polymerase were used as well as Invitrogen's PCR SuperMix High Fidelity. PCRs were carried out with an MJ Research PTC-200 Peltier Thermal Cycler. Synthetic oligonucleotides were made by Integrated DNA Technologies. For cloning, plasmids were transformed into *E. coli* strain DH5α (F⁻ φ80*lac*ZΔM15 Δ(*lac*ZYA-*arg*F)U169 *deo*R *rec*A1 *end*A1

*hsd*R17(r_k^-, m_k^+) *pho*A *sup*E44 *thi*-1 *gyr*A96 *rel*A1 λ^-) with a standard heat shock

protocol (*S1*), and isolated with Qiagen QIAprep Spin Miniprep Kits. Plasmid

modifications were confirmed by restriction digests and sequencing by Agencourt.

2. RTC Counter Plasmid Design

Two plasmids – the RTC 2-Counter (Fig. S1) and RTC 3-Counter (Fig. S2) – were made,

both derived from the riboregulator vector pZER21Y12α12G reported by Isaacs *et al.* (*4*),

itself based strongly on the Lutz and Bujard pZE21 expression vector (*S2*). These contain

kanamycin resistance, ColE1 origin of replication, the P_{BAD} promoter driving

transcription of taRNA version taR12 (*4*), and the $P_{Ltet0-1}$ promoter. Both constructs were

modified to have the $P_{Ltet0-1}$ promoter driving transcription of T7 RNA polymerase

(NCBI Accession NC_001604.1). For the RTC 2-Counter construct, there is also the T7

promoter (TAATACGACTCACTATAGGGAGA) driving transcription of GFPmut3b;

for the RTC 3-Counter construct, the T7 promoter drives transcription of T3 RNA

polymerase (NCBI Accession NC_003298.1). The RTC 3-Counter additionally contains

the T3 promoter 14.3m (ATTAACCCTCACTAAAGGGAGA) (*S3*), which drives

transcription of GFPmut3b. All genes used in these constructs were engineered with the

crR12 *cis*-repressor sequence upstream of the RBS (*4*). All promoters were paired with

appropriate transcription terminators: P_{BAD} with the *E. coli* rrnB terminator, $P_{Ltet0-1}$ with

the *E. coli* terminator T1 (of the rrnB terminator), P_{T7} with T7 transcription terminator

Tphi, and P_{T3} with T3 transcription terminator Tphi.

3. RTC Counter Experimental Conditions

All experiments were conducted with the *E. coli* K-12pro strain (F$^+$, P$_{N25}$/tetR, P$_{laciq}$/lacI, Sp^r). For both the RTC 2-Counter and 3-Counter experiments, cells containing the counting vector were grown overnight in a Luria-Bertani (DIFCO) medium containing 30 µg/mL kanamycin, then diluted 1:100 and grown between 5 and 6.5 hours to an OD between 1.1 and 1.6 before being aliquoted into clear-bottom 24-well assay plates, 1mL per well. For the 2-Counter data shown in Figs. 1B and S3A, cells pulsed with arabinose had arabinose added to their wells for a final concentration of 0.001% at 0 minutes (immediately following the aliquot) and/or at 50 minutes. Pulses were left in the media for 10 minutes before cells were transferred into 1.5 mL tubes and spun for 1 minute at 8,000 rpm. Media was aspirated out of these tubes, and cells were resuspended in fresh media and transferred back to the plate. The 3-Counter experiments had 0.01% (final concentration) arabinose pulses delivered at varying times. All cells in 24-well plates were maintained at 37°C throughout the course of the experiments, with shaking in between measurements. Experiments were performed in triplicate, and all data points shown are the mean values of these replicates.

4. RTC Counter Flow Cytometer Measurements

Data for Figs. 1B and 1D were collected with a Becton Dickinson FACSCalibur flow cytometer. Fluorescence was calibrated with Calibrite Beads (Becton Dickinson) and measured with a 488-nm argon laser excitation and a 515-nm to 545-nm emission filter. At each time point, 8 µL of cells were taken from the plate wells and diluted into 1 mL of filtered PBS, pH 7.2. Mean fluorescence measurements were calculated by BD

Biosciences' Cellquest Pro software, from samples containing at least 100,000 cells. No filters or gates were used on the cell populations.

5. RTC Counter Spectrophotometer Measurements

Data for Fig. S3 was collected with a Tecan SPECTRAFluor Plus spectrophotometer. Excitation and emission wavelengths were 485nm and 535nm, respectively, with a fixed gain set at 40.

6. RTC Counter Mathematical Modeling

Mathematical modeling was used to verify the logic-based predictions of our design, to investigate the effects of pulse frequency and pulse length on the performance of the RTC counters, and to explore the possibility of counting to higher numbers. We used ordinary differential equations (ODE) to describe the temporal trajectories of population averages for all biochemical species. Stochastic modeling was not included because of the population homogeneity demonstrated in Fig. S4. Details for the modeling of each of the two constructs are explained in the sections below.

6.1. The RTC 2-Counter Model

Based on the design of the RTC 2-Counter, we approximated the system dynamics using the following biochemical reactions:

$$\phi \underset{d\_taRNA}{\overset{s\_taRNA}{\rightleftharpoons}} taRNA \tag{1}$$

$$\phi \underset{d\_mT7}{\overset{s0\_mT7}{\rightleftharpoons}} mT7cr \tag{2}$$

$$\phi \xrightleftharpoons[d\_mGFP]{s\_GmRNA} mGFPcr \tag{3}$$

$$mT7cr + taRNA \xrightleftharpoons[kb1]{kf1} mT7 \tag{4}$$

$$mGFPcr + taRNA \xrightleftharpoons[kb2]{kf2} mGFP \tag{5}$$

$$mT7 \xrightarrow{sT7} mT7 + pT7 \tag{6}$$

$$mGFP \xrightarrow{sGFP} mGFP + pGFP \tag{7}$$

$$pT7 \xrightarrow{d\_pT7} \phi \tag{8}$$

$$pGFP \xrightarrow{d\_pGFP} \phi \tag{9}$$

where Eqs. (1)-(3) represent the synthesis and degradation of trans-activator (*taRNA*), T7 RNA polymerase transcripts in cis-repressed form (*mT7cr*), and GFP transcripts in cis-repressed form (*mGFPcr*), respectively. Transcripts in cis-repressed form are indicated by "cr". Kinetic parameters are as indicated in the equations. Eqs. (4) and (5) represent the binding of *taRNA* with *mT7cr* and *mGFPcr* so that the transcripts can be translated; these repression-relieved transcripts are denoted as *mT7* and *mGFP*. Eqs. (6) and (7) represent the translations of *mT7* and *mGFP*, respectively, with *pT7* and *pGFP* as notations for these two proteins. Finally, Eqs. (8) and (9) represent the degradation of proteins. As shown in Fig. 2A of the main text, these biochemical reactions were sufficient to describe the system dynamics with high accuracy.

Based on these reactions, we wrote down the differential equations that describe the temporal evolution of all the species. Some of the parameters in the biochemical reactions are lumped parameters that are expanded to their explicit forms in the differential equations. The notations for all chemical species in this model (and the RTC 3-Counter

model) are simplified and listed in Table S1, with all parameter values listed in Table S2. The square brackets in these equations indicate chemical species concentration. Because the fluorescence data to which we directly fit the model (see below for details) have arbitrary units, GFP protein concentrations in the model are considered nondimensional. All other parameter values, except for degradation rates (min^{-1}) and k_ara (concentration), are nondimensional as well. The following five equations were used to capture the temporal dynamics of the system:

$$\frac{d[taRNA]}{dt} = sT \frac{[ara]}{[ara]+k\_ara} + s0\_taRNA - d\_taRNA \cdot [taRNA] \qquad (10)$$

$$\frac{d[mT7cr]}{dt} = s0\_mT7cr - d\_mT7cr \cdot [mT7cr] \qquad (11)$$

$$\frac{d[pT7]}{dt} = s_0\_pT7 \cdot [mT7cr] + s\_pT7k \cdot [taRNA] \cdot [mT7cr] - d\_pT7 \cdot [pT7] \quad (12)$$

$$\frac{d[mGFPcr]}{dt} = s0\_mGFPcr + k\_pT7 \cdot \frac{[pT7]^n}{km7^n + [pT7]^n} - d\_mGFP \cdot [mGFPcr] \quad (13)$$
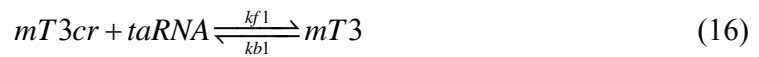
$$\frac{d[pGFP]}{dt} = s_0\_pGFP \cdot [mGFPcr] + s\_pGFPk \cdot [taRNA] \cdot [mGFPcr]$$
$$-d\_pGFP \cdot [pGFP] \qquad (14)$$

where on the right-hand side of Eq. (10), taRNA synthesis rate has two parts: the first part (sT*[ara]/([ara]+kara)) represents the synthesis rate induced by arabinose and the second part (s_0_taRNA) represents the basal production rate without any induction,. To simplify the system, we assumed that the arabinose induction effect has a Hill function form with a Hill coefficient equal to 1. The third term of Eq. (10) represents taRNA

degradation using a simple exponential decay with rate *d_taRNA*. In Eq. (11), cis-repressed T7 RNA polymerase transcripts (*mT7cr*) are constitutively expressed, with a constant production rate (*s0_mT7cr*) and exponential decay. Similarly, in Eq. (12), T7 RNA polymerase protein synthesis rate has two parts: $s_0\_pT7*[mT7cr]$ represents the translation rate of *mT7cr* without *taRNA* binding, and *s_pT7k*[taRNA]*[mT7cr]* represents the translation rate of *mT7cr* with *taRNA* binding. Here we assumed that *taRNA* binding and dissociation with mRNA [Eqs. (4) and (5)] have a much faster time scale than other reactions and reach equilibrium instantly. Thus, the parameter *s_pT7k*, for example, is also a lumped parameter with information about the binding reaction in Eq. (4) included. In Eq. (13), GFP mRNA synthesis depends on the basal transcription rate and on T7 RNA polymerase protein abundance. We used a general Hill function to describe this dependency: $k\_pT7*[pT7]^n/([pT7]^n+[km7]^n)$, where *n* accounts for any type of cooperativity caused by T7 RNA polymerase activation. In Eq. (14), GFP protein dynamics parallel that of the T7 RNA polymerase protein in Eq. (12).

6.2. Extension to the RTC 3-Counter

The RTC 3-Counter construct is similar to the RTC 2-Counter in design and topology (Fig. 1C of main text), and they have a number of components in common. So for the RTC 3-Counter model we used many of the same equations used for the RTC 2-Counter model. Besides the reactions in Eqs. (1)-(9), there are four additional reactions:

$$\phi \underset{d\_mT3}{\overset{s\_T3mRNA}{\rightleftharpoons}} mT3cr \tag{15}$$

$$mT3cr + taRNA \underset{kb1}{\overset{kf1}{\rightleftharpoons}} mT3 \tag{16}$$

$$mT3 \xrightarrow{\ sT3\ } mT3 + pT3 \tag{17}$$

$$pT3 \xrightarrow{\ d\_pT3\ } \phi \tag{18}$$

where Eq. (15) represents the synthesis and degradation of cis-repressed T3 RNA polymerase transcripts (*mT3cr*) and Eq. (16) represents the binding of *taRNA* with *mT3cr*. Eqs. (17) and (18) represent translation and degradation of T3 RNA polymerase protein, respectively. The differential equations describing the RTC 3-Counter construct are similar to the RTC 2-Counter differential equations, except Eq. (13) changes to:

$$\frac{d[mGFPcr]}{dt} = s0\_mGFPcr + k\_pT3 \cdot \frac{[pT3]^n}{km3^n + [pT3]^n} - d\_mGFP \cdot [mGFPcr] \tag{19}$$

and the following two equations are added:

$$\frac{d[mT3cr]}{dt} = s0\_mT3cr + k\_pT7 \cdot \frac{[pT7]^n}{km7^n + [pT7]^n} - d\_mT3 \cdot [mT3cr] \tag{20}$$

$$\frac{d[pT3]}{dt} = s_0\_pT3 \cdot [mT3cr] + s\_pT3k \cdot [taRNA] \cdot [mT3cr] - d\_pT3 \cdot [mT3cr] \tag{21}$$

Eqs. (20) and (21) describe the change of T3 RNA polymerase transcripts and proteins over time. They have the same forms as Eqs. (13) and (14), respectively, with similar parameter implications.

6.3. RTC Counter Arabinose Induction

Different counter strains were induced by different numbers of external arabinose pulses to test and verify the counting behavior. To account for the arabinose pulse dynamics, we modeled it with two differential equations. The first equation describes arabinose when it is present in the medium:

$$\frac{d[ara]}{dt} = -cAra \tag{22}$$

This represents a constant consumption rate of arabinose, when it is present in abundance. The second equation describes arabinose after the cells have been spun and resuspended in arabinose-free media. The leftover, mainly intracellular arabinose is modeled as an exponentially decaying chemical species:

$$\frac{d[ara]}{dt} = -dAra \cdot [ara] \tag{23}$$

In the simulations, Eqs. (22) and (23) were used alternately so as to be consistent with actual experimental conditions.

6.4. RTC Counter Fitting of Experimental Data

Matlab function *lsqcurvefit* was used to narrow down the model parameters by fitting the model equations to experimental measurements. The parameter set that resulted in the optimal data fitting among two hundred runs was chosen as the set for Fig. 2 of the main text, with fluorescence levels of uninduced samples subtracted from all other experimental data. Parameters values used for these figures are listed in Table S2. The experimental arabinose doses used in the RTC 3-Counter experiments were ten-fold higher than those in the RTC 2-Counter experiments; thus parameters *k_ara* and *cAra*

were adjusted ten-fold higher (as written in Table S2) for the RTC 3-Counter model to match the experimental results.

7. DIC Counter Plasmid Construction

DIC Counter plasmids were constructed using basic molecular cloning techniques (*S1*). New England Biolab's restriction endonucleases, T4 DNA Ligase, and NEB's Phusion PCR kits were used. PCRs were carried out with an MJ Research PTC-200 Peltier Thermal Cycler. Synthetic oligonucleotides were made by Integrated DNA Technologies. Single-inducer DIC Counter plasmids were transformed into *E. coli* strain DH5α (F$^-$ φ80*lac*ZΔM15 Δ(*lac*ZYA-*arg*F)U169 *deo*R *rec*A1 *end*A1 *hsd*R17(r_k^-, m_k^+) *pho*A *sup*E44 *thi*-1 *gyr*A96 *rel*A1 λ$^-$).   Multiple-inducer DIC Counter plasmids were transformed into *E. coli* strain DH5αPRO (F$^-$ φ80*lac*ZΔM15 Δ(*lac*ZYA-*arg*F)U169 *deo*R *rec*A1 *end*A1 *hsd*R17(r_k^-, m_k^+) *pho*A *sup*E44 *thi*-1 *gyr*A96 *rel*A1 λ$^-$, P_{N25}/tetR, P_{laciq}/lacI, Sp^r). Transformations were carried out using standard electroporation protocols (*S1*) and isolated with Qiagen QIAprep Spin Miniprep Kits. Plasmid modifications were confirmed by restriction digests.

8. DIC Counter Plasmid Design

The single-inducer DIC 2-Counter (Fig. S8) and 3-Counter (Fig. S9) and multiple-inducer DIC 3-Counter (Fig. S10) were based on the single-copy pBAC platform (*9*). pBAC-lacZ (Addgene plasmid 13422) was obtained from Addgene (Cambridge, MA). We cloned all components for the DIC Counters in between ScaI and PciI restriction sites

in pBAC-lacZ. Custom sequences, including recombinase recognition sites, were constructed using sequential PCR with DNA obtained from Integrated DNA Technologies (Coralville, IA). Promoters $P_{Ltet0-1}$ and P_{A1lacO} and terminators were obtained from Ref. *S2*, while P_{BAD} was obtained from Ref. *4*. The *cre* gene was obtained from Ref. *20*. The *flp$_e$* gene was derived from pCAG-Flpe (Addgene plasmid 13787) and based on Ref. *S4*. The ribosome-binding sequences used in each stage were derived from Ref. *12*, while *ssrA*-based degradation tags were designed according to Ref. *S5*.

9. DIC Counter Experimental Conditions

All experiments were performed in Luria-Bertani media containing 30 μg/mL kanamycin. Prior to performing flow cytometer measurements on the DIC Counters, cells were grown overnight. To initiate experiments, cells were diluted 1:2000 in fresh media and grown at 37°C and 300 rpm with inducers as indicated in the specific figures. Inducer concentrations were anhydrotetracycline = 700 ng/mL, arabinose = 0.1%, and IPTG = 10 mM except for Fig. 4B in which anhydrotetracycline = 100 ng/mL, arabinose = 10^{-3}%, and IPTG = 10 mM. At all inducer transitions (i.e., transitions from media with inducer to media without inducer, transitions from media without inducer to media with inducer, or transitions from media with one inducer to media with another inducer), cells were diluted 1:2000 in fresh media. Only in Fig. 3C with pulse intervals 2h and 4h were cells not diluted 1:2000 in fresh media for transitions from media without inducer to media with inducer due to low optical density of the cultures. Instead, inducer was added directly to the media; however, cells were still diluted 1:2000 in fresh media for transitions from media with inducer to media without inducer.

10. DIC Counter Flow Cytometer Measurements

Data for Figs. 3, 4, S11, S12, and S13 were collected with a Becton Dickinson FACSCalibur flow cytometer. Fluorescence was calibrated with Calibrite Beads (Becton Dickinson) and measured with a 488-nm argon laser excitation and a 515-nm to 545-nm emission filter. Before analysis, cells were diluted in sterile phosphate-buffered saline. Becton Dickinson Calibrite Beads were used for instrument calibration. 50,000 cells were collected for each sample, gated to ensure consistency between samples, and processed with MATLAB to calculate mean fluorescence data points (Mathworks, Natick, MA).

SOM Text

1. RTC Counter Characteristics and Improvements

1.1. Whole Population Measurements

To verify the counting behavior, we also analyzed the RTC 2-Counter and the RTC 3-Counter with a spectrophotometer, which measures the total fluorescence in a given cell population. These spectrophotometer results (Figs. S3A and S3B) corroborate the data from the flow cytometer (Figs. 1B and 1D). In the case of the RTC 2-Counter (Fig. S3A), the uninduced population similarly shows no increase in fluorescence, while populations that received either the first or the second arabinose pulse exhibit only some fluorescence. Cells that receive both pulses show a striking increase in fluorescence at 50 minutes, validating our design. The spectrophotometer measurements of the RTC 3-Counter reveal

a similar corroboration, in which only cells that are pulsed three times respond with sharp increases in fluorescence.

Flow cytometer and spectrophotometer data sets do diverge qualitatively, where flow cytometer measurements exhibit a peak in fluorescence and then decrease whereas spectrophotometer measurements exhibit a fluorescence plateau. The decrease is likely due to external factors such as cell division (*S6*), and is revealed in single-cell measurements of the flow cytometer. This effect is not seen in the spectrophotometer, where measurements are made on whole populations. Data presented in Figs. S3A and S3B are the mean of three replicates, and smoothed with a rolling window average.

1.2. Flow Cytometry Population Analysis

The data presented in Figs. 1B and 1D are mean fluorescence values of RTC counter cell populations, measured by a flow cytometer. In Fig. S4, we show the fluorescence profile of the entire RTC 3-Counter population when it is uninduced, after the second pulse, and after the third pulse. It is clear that the entire population shifts homogeneously following induction, with the greatest shift occurring as a result of the third pulse.

1.3. Verification of Discrete Counting

To verify that the counting response is driven by discrete induction pulses and not simply a summation of induction length, we took a fixed total length of induction and split it into two and three pulses. RTC 3-Counter cells were either given two short pulses followed by a long pulse or two long pulses, with total induction time equal for both sets of cells

(Fig. S5 inset). It can be seen in Fig. S5 that cells receiving three pulses (blue) generate

significantly more GFP than cells receiving two pulses (red), demonstrating a true

counting mechanism and not simply a summing effect. This supports our claim that the

counter is able to distinguish between different numbers of pulses, even when total

induction time is held constant. Additionally, our mathematical model accurately

predicted the experimental results for both scenarios.

1.4. Higher Number Counters

To investigate the possibility of expanding our design to count higher numbers, we

hypothetically expanded our system using mathematical modeling. We added extra genes

to the cascade, each one an RNA polymerase whose downstream promoter regulates the

transcription of the gene at the next node. We modeled cascades with up to ten nodes; in

each case the first node is T7 RNA polymerase, the last node is GFP, and all nodes in

between are polymerases with exactly the same kinetic properties as T3 RNA polymerase.

With two additional differential equations for each node, we use mathematical modeling

to predict the behavior of these higher number counters by comparing the fluorescence

readout of n, n-1, and n-2 arabinose pulses for each n-node counter. As shown in Fig.

S6A, the red line is the fluorescence result of n pulses, the green line of n-1 pulses, and

the blue line n-2 pulses. It can be seen that the absolute difference in fluorescence levels

between n and n-1 pulses increases with cascade length, suggesting the design can better

distinguish different numbers of pulses as it is extended. Additionally, all three lines

increase as the construct is extended, due to signal propagation and the accumulation of long-lived proteins as more pulses are delivered.

This predicted accumulation effect results in the failure of this system to perform digitally as *n* increases, with ones and zeros no longer represented by high and low protein concentrations. However, by examining the temporal dynamics of all the chemical species in the cascades, we identified that it is the long half-life of GFP protein that causes the signal increase after *n*-1 and *n*-2 pulses. Figure S6B is the predicted counter output in which GFP protein has its half-life shortened to 8 minutes instead of the 231 minute half life used for Fig. S6A. Figure S6B illustrates that when the final output protein has a shortened half-life, the counter performance is remarkably robust as *n* increases. Counting from 2 to 10, output from *n* pulses increases almost exponentially while output from *n*-1 and *n*-2 pulses increases only marginally.

If shortening the final protein's half-life is not possible or desirable, an alternative method for digitizing the output signal would be to couple the counter to a toggle switch (12). By placing one of the toggle repressor proteins at the final node of the counter cascade, it would be possible to flip a toggle from one state to the other with expression from the counter. The sharp and tunable switching threshold of a toggle switch may be used to filter out counter leakage due to *n*-1 or *n*-2 pulses, switching states only when *n* pulses produces a concentration of repressor proteins in excess of the switching threshold.

2. Extending the DIC Counter

Each of our individual counting units requires only a single recombinase whereas the protein-based toggle switch utilizes two proteins (*12*). This allows our design to be extendable in a modular fashion using >100 identified recombinases to count to higher numbers (*6*). Recombinases can also be mutagenized to have altered site preferences or thermostabilities, allowing for increased diversity to create synthetic gene circuits. The availability of additional recombinases enables the DIC counter to be extended more readily than other systems that require rarer or more specialized components.

3. RTC and DIC Counter Designs: Possible Improvements

Compared to electronic counters, our biological counters are in an early stage of development and have some distinct limitations. Our counters scale linearly instead of exponentially as is the case with digital electronic circuits that count in binary (*S7*). Counter designs which count in binary require the addition of bit reset and carry operations (*S7*). The DIC counter is amenable to being adapted with advanced digital designs due to the ability of SIMMs to maintain memory and invert in both orientations. Reset operations could be carried out by downstream promoters which drive the transition of inverted SIMMs back to their original orientations. Carry operations could be achieved by components that act in *trans* to affect DNA orientation, insertions, or deletions on many different SIMMs or DIC counters; these *trans*-based components may include bacteriophage integrases and excisionases (*6*) or transcriptional activators. Future development of biological counters with exponential scaling will greatly expand the potential applications of biological counters.

An additional limitation of our counters is their inability to detect very high frequency inputs. Though there will invariably be upper limits to pulse frequencies that can be detected by counters, those limits may be improved by combining synthetic counters with pulse-generating circuits that can detect edge transitions with greater rapidity and/or with amplifiers that can enhance the magnitude of inputs. Pulse-generating circuits may also enable the RTC counter and the single-inducer DIC counter to record low-frequency events with greater fidelity.

Supplementary Figure Captions

Fig. S1. The RTC 2-Counter plasmid. Genes are denoted by arrows within the plasmid circle, promoters by arrows on the plasmid circle, transcriptional terminators by red rectangles, taRNA by a green rectangle, and origin by a blue rectangle.

Fig. S2. The RTC 3-Counter plasmid. Genes are denoted by arrows within the plasmid circle, promoters by arrows on the plasmid circle, transcriptional terminators by red rectangles, taRNA by a green rectangle, and origin by a blue rectangle.

Fig. S3. Spectrophotometer measurements of RTC 2-Counter and RTC 3-Counter fluorescence over time. (**A**) Spectrophotometer measurements show total population fluorescence of cells containing the RTC 2-Counter construct. Experimental conditions match exactly those used for Fig. 1B. (**B**) Spectrophotometer measurements of cells containing the RTC 3-Counter construct, with experimental conditions matching exactly those used for Fig. 1D.

Fig. S4. A histogram of cell counts and fluorescence in RTC 3-Counter cells. Shown in red is a population of uninduced cells, in green cells that have been pulsed twice, and in blue cells that have been pulsed three times.

Fig. S5. The RTC 3-Counter response to varying length pulses. The counter is induced by two sets of arabinose pulses, displayed as blue and red bars in the figure inset. With 20 minute intervals between all pulses, the first set (in blue) is induced for 11 minutes, then 11 minutes again, then 22 minutes. The second set (in red) is induced by two 22 minute pulses. Experimental data, plotted as a mean fluorescence value for cell populations as measured by flow cytometry, is represented by circles. The blue and red lines are mathematical model predictions corresponding to the pulse patterns in the inset.

Fig. S6. Model predictions of the fluorescence output of n-node RTC Counters in response to n, n-1, and n-2 arabinose pulses. (**A**) The numbers on the x-axis represent counters with n nodes, and for each counter we plot the fluorescence output due to n, n-1, and n-2 pulses. We use our best-fit parameter values in this figure, the same as those used for Fig. 2. (**B**) This is similar to Fig. S6A, except that GFP protein half-life has been reduced from 231 minutes to 8 minutes.

Fig. S7. Abstract design of the Single Invertase Memory Modules (SIMMs) used in the DIC counters. The SIMMs are composed of opposing recombinase recognition sites (R_f and R_r) which contain between them an inverted promoter (P_{inv}), a synthetic ribosome-binding-sequence (RBS), a recombinase gene (*rec*), an *ssrA*-based degradation tag, and a transcriptional terminator (Term). The SIMM maintains memory based on its DNA orientation, which can be inverted when the recombinase is expressed.

Fig. S8. The single-inducer DIC 2-Counter plasmid. Genes are denoted by arrows within the plasmid circle, promoters by arrows on the plasmid circle, transcriptional terminators by red rectangles, *ssrA*-based degradation tags by brown rectangles, and recombinase recognition sites by rectangles of other colors.

Fig. S9. The single-inducer DIC 3-Counter Plasmid. Genes are denoted by arrows within the plasmid circle, promoters by arrows on the plasmid circle, transcriptional terminators by red rectangles, *ssrA*-based degradation tags by brown rectangles, and recombinase recognition sites by rectangles of other colors.

Fig. S10. The multiple-inducer DIC 3-Counter Plasmid. Genes are denoted by arrows within the plasmid circle, promoters by arrows on the plasmid circle, transcriptional terminators by red rectangles, *ssrA*-based degradation tags by brown rectangles, and recombinase recognition sites by rectangles of other colors.

Fig. S11. The single-inducer DIC 2-Counter construct design and results. **(A)** The single-inducer DIC 2-Counter is characterized by a single Single Invertase Memory Module (SIMM) with P_{BAD} as the inducible upstream promoter and inducible inverted promoter within the SIMM. **(B)** Mean fluorescence of single-inducer DIC 2-Counter cell populations over time, measured by a flow cytometer, demonstrates a significant increase in GFP fluorescence after exposure to two pulses of arabinose. **(C)** Mean fluorescence of single-inducer DIC 2-Counter cell

populations over time, measured by a flow cytometer, demonstrates that cells grown with no inducer for 9 hours followed by a single pulse of arabinose lasting 7 hours did not show significant GFP expression. Mean fluorescence was normalized against the maximum fluorescence for cells obtained in Figs. S11B and S11C in order to allow comparison between the two plots.

Fig. S12. Flow cytometry population data for the single-inducer DIC 3-Counter exposed to zero, one, two, or three pulses of arabinose. Each arabinose pulse was 8 hours long and spaced by 9 hours of no arabinose exposure. The data demonstrate that there is no leakage with one pulse ("Ara" in the legend), a small degree of leakage with two pulses ("Ara => Ara" in the legend), and a large degree of activation after three pulses ("Ara => Ara => Ara" in the legend).

Fig. S13. Switching times for each SIMM stage in the multiple-inducer DIC 3-Counter were examined by varying the length of exposure to either anhydrotetracycline or arabinose while holding all other inputs constant (aTc followed by Ara followed by IPTG). When not being varied, aTc and Ara pulses were 18 hours in duration and IPTG pulses were 12 hours in duration. The last input to the multiple-inducer DIC 3-Counter, IPTG, does not drive an invertase stage and directly induces the transcriptional GFP output of the system. **(A)** The first SIMM stage responds to aTc within 6 hours of exposure. Very long aTc exposure times did not result in increased GFP fluorescence. **(B)** The second SIMM stage begins to respond to

Ara within 9 hours of exposure. Very long arabinose exposure times did not result

in increased GFP fluorescence.

SOM Tables

Table S1. A summary of chemical species represented in the RTC Counter model and their notations.

Notation	Chemical species
taRNA	*trans*-activator
mT7cr	*cis*-repressed T7 RNA polymerase mRNA
mT7	T7 RNA polymerase mRNA
pT7	T7 RNA polymerase protein
mGFPcr	*cis*-repressed GFP mRNA
mGFP	GFP mRNA
pGFP	GFP protein
mT3cr	*cis*-repressed T3 RNA polymerase mRNA
mT3	T3 RNA polymerase mRNA
pT3	T3 RNA polymerase protein
ara	Arabinose

Table S2. A list of all parameter values used in the RTC Counter models.

k_ara* concentration	0.0571	d_pT7	0.0056	km7	3.0455
s0_taRNA	0.0008	s_pGFPk	0.9923	k_pT3	3.006
d_taRNA	0.1177	d_pGFP	0.003	s0_mT3cr	0.0003
s0_mT7cr	0.0252	dAra leftover decaying	0.1201	d_mT3	0.0701
d_mT7	0.0706	s0_pT7	0.0003	s0_pT3 inital amount	0
k_pT7	3.8009	s0_pGFP	0.1007	s_pT3k	0.0115

s0_mGFPcr	0.0123	sT	0.8467	d_pT3	0.0069
d_mGFP	0.07	cAra* constant consumptionrate	0.0003	n3	0.8892
s_pT7k	0.0766	n7	2.602	km3	7.9075

SOM References

S1. J. Sambrook, E. F. Fritsch, T. Maniatis, *Molecular Cloning: A Laboratory Manual*, (Cold Spring Harbor Laboratory Press, Plainview, New York, edn. 2, 1989).

S2. R. Lutz, H. Bujard, *Nucleic Acids Res* **25**, 1203 (1997).

S3. D. Sengupta, D. Chakravarti, U. Maitra, *J Biol Chem* **264**, 14246 (1989).

S4. F. Buchholz, P. O. Angrand, A. F. Stewart, *Nature biotechnology* **16**, 657 (Jul, 1998).

S5. J. B. Andersen et al., *Appl Environ Microbiol* **64**, 2240 (Jun, 1998).

S6. J. Roostalu, A. Joers, H. Luidalepp, N. Kaldalu, T. Tenson, *BMC Microbiol.* **8**, 68 (2008).

S7. P. Horowitz, W. Hill, *The Art of Electronics*. (Cambridge University Press, Cambridge, United Kingdom, ed. 2nd, 1989).

Figure S1
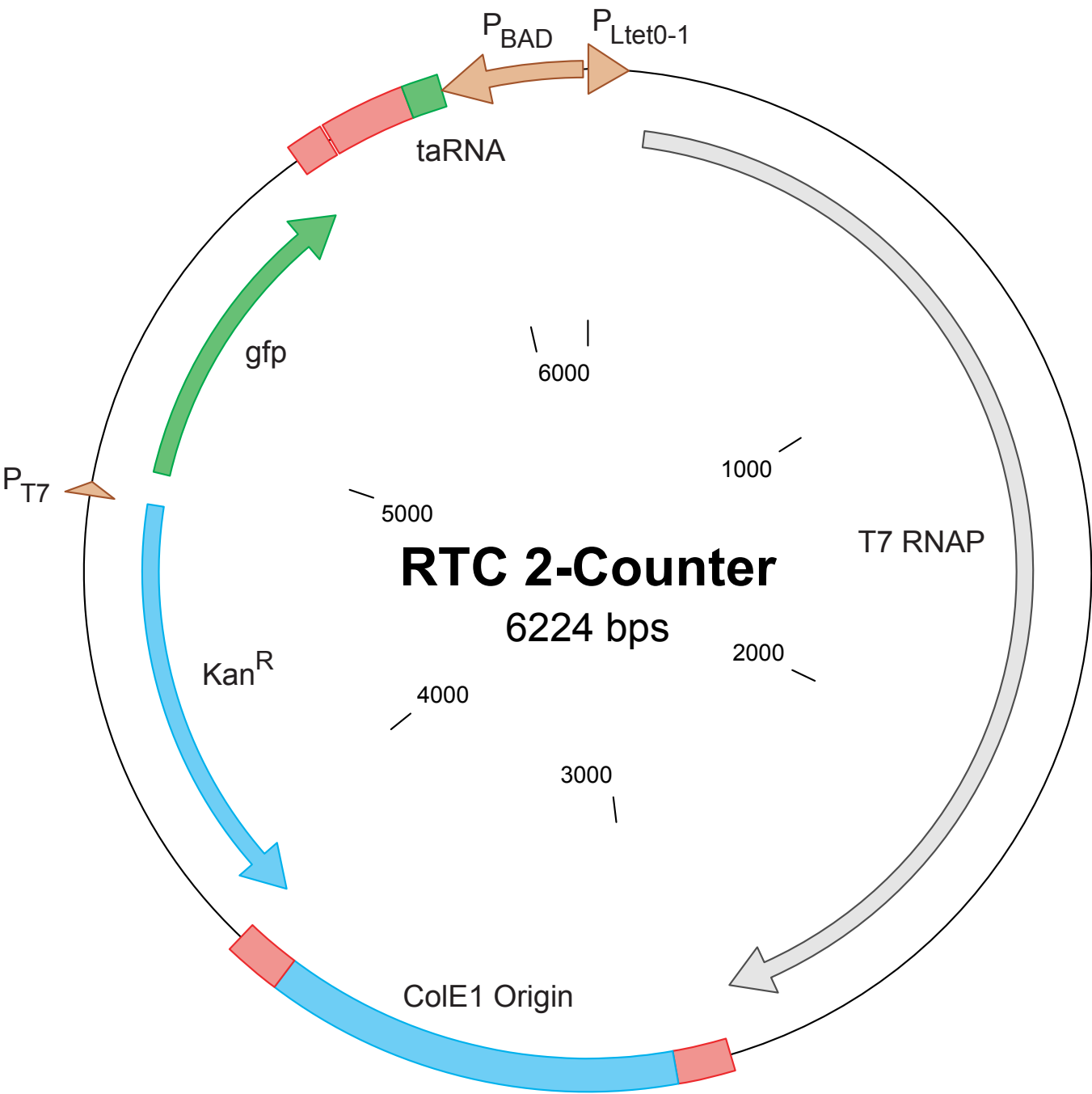
Figure S2
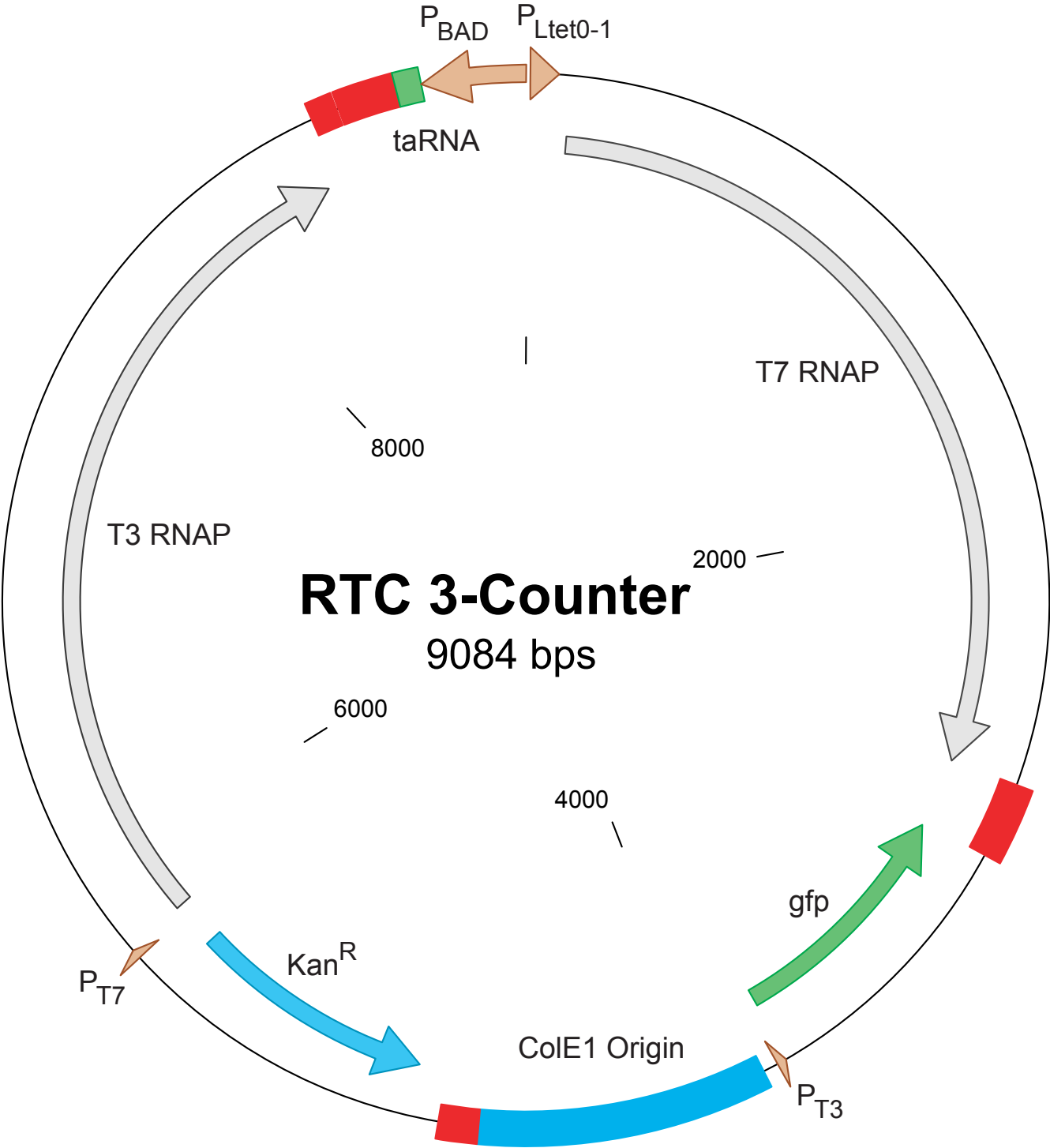
Figure S3
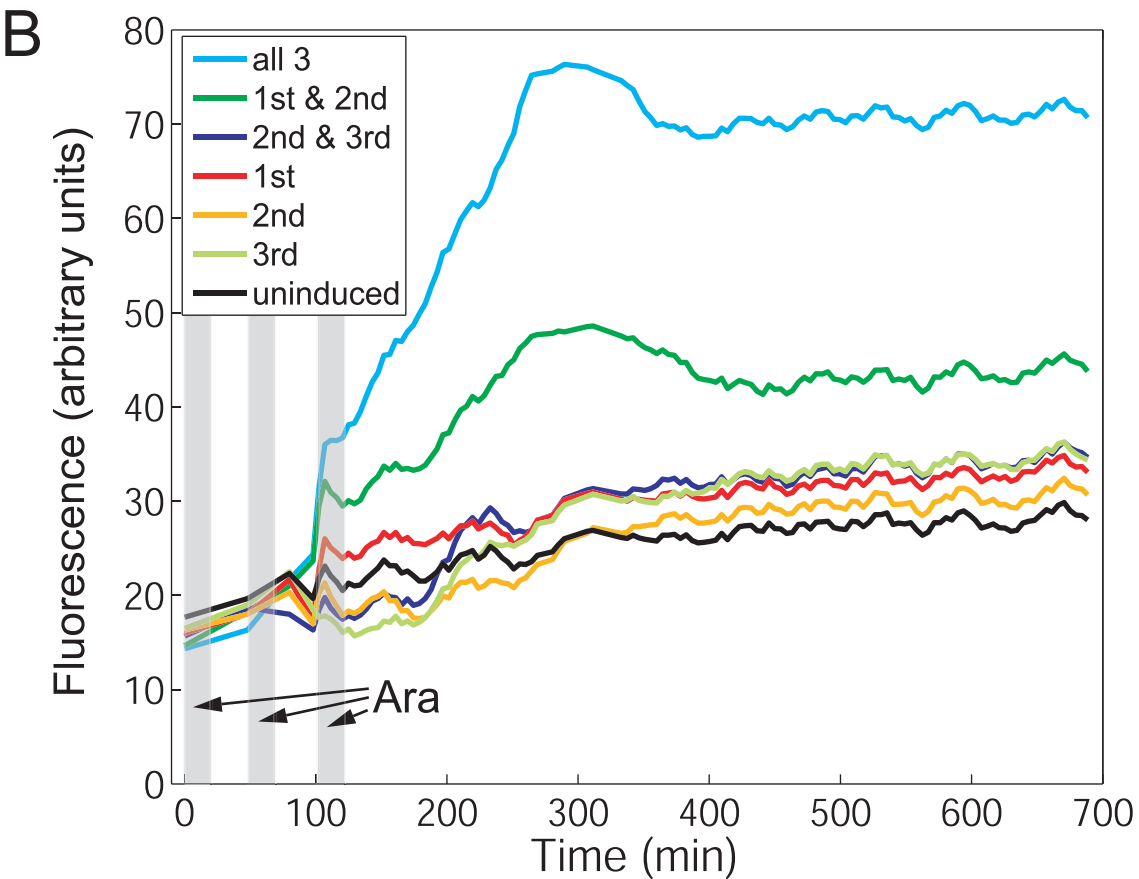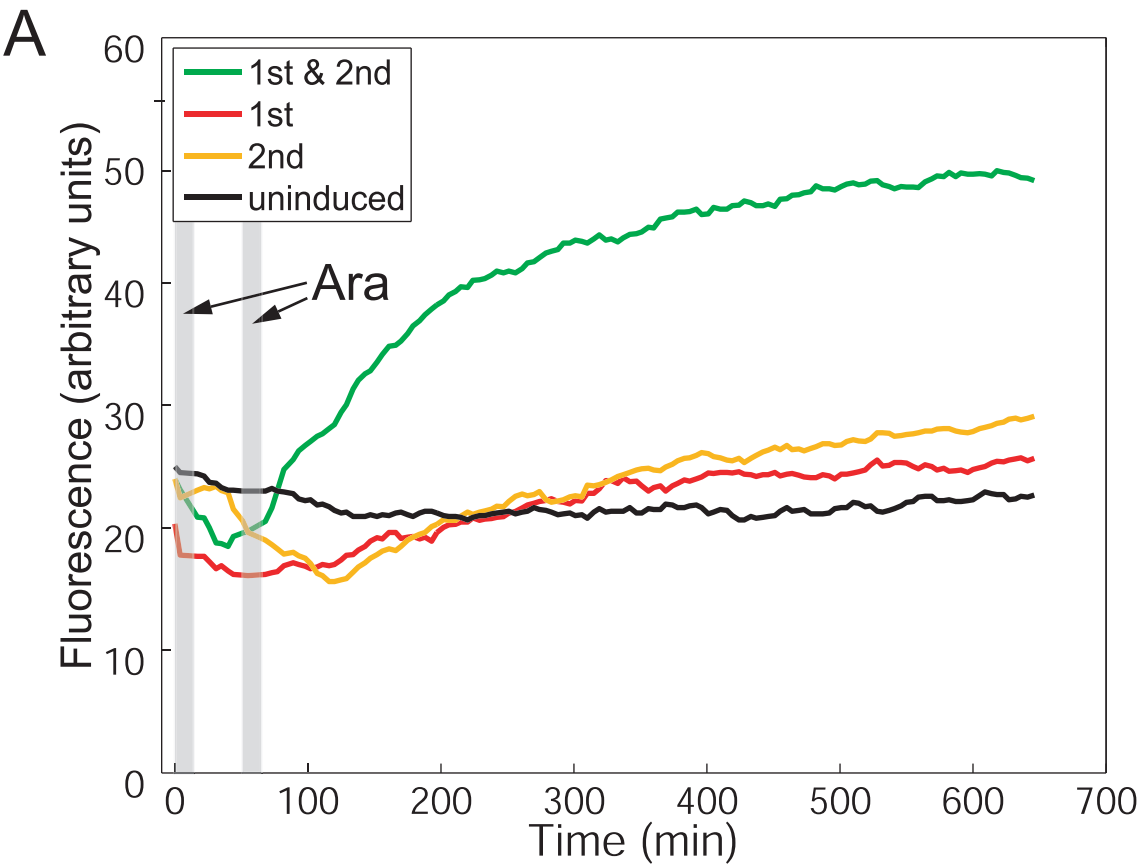
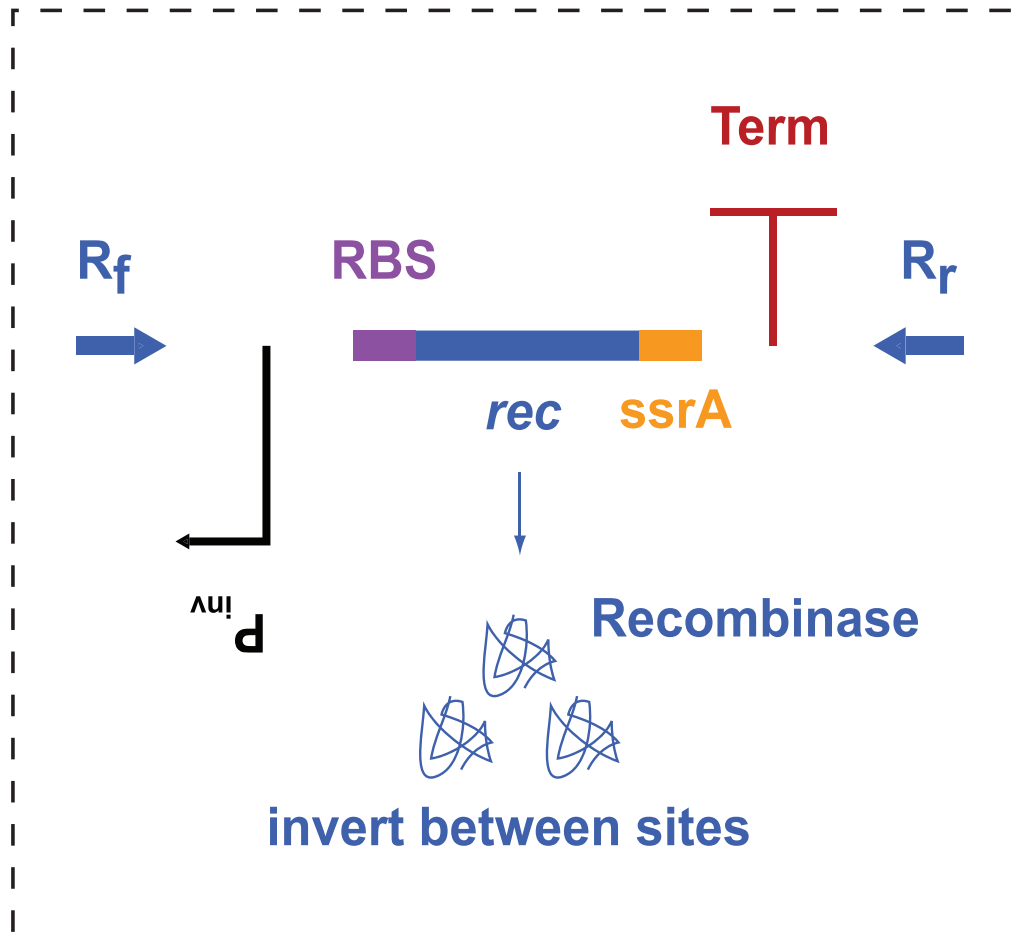Figure S4
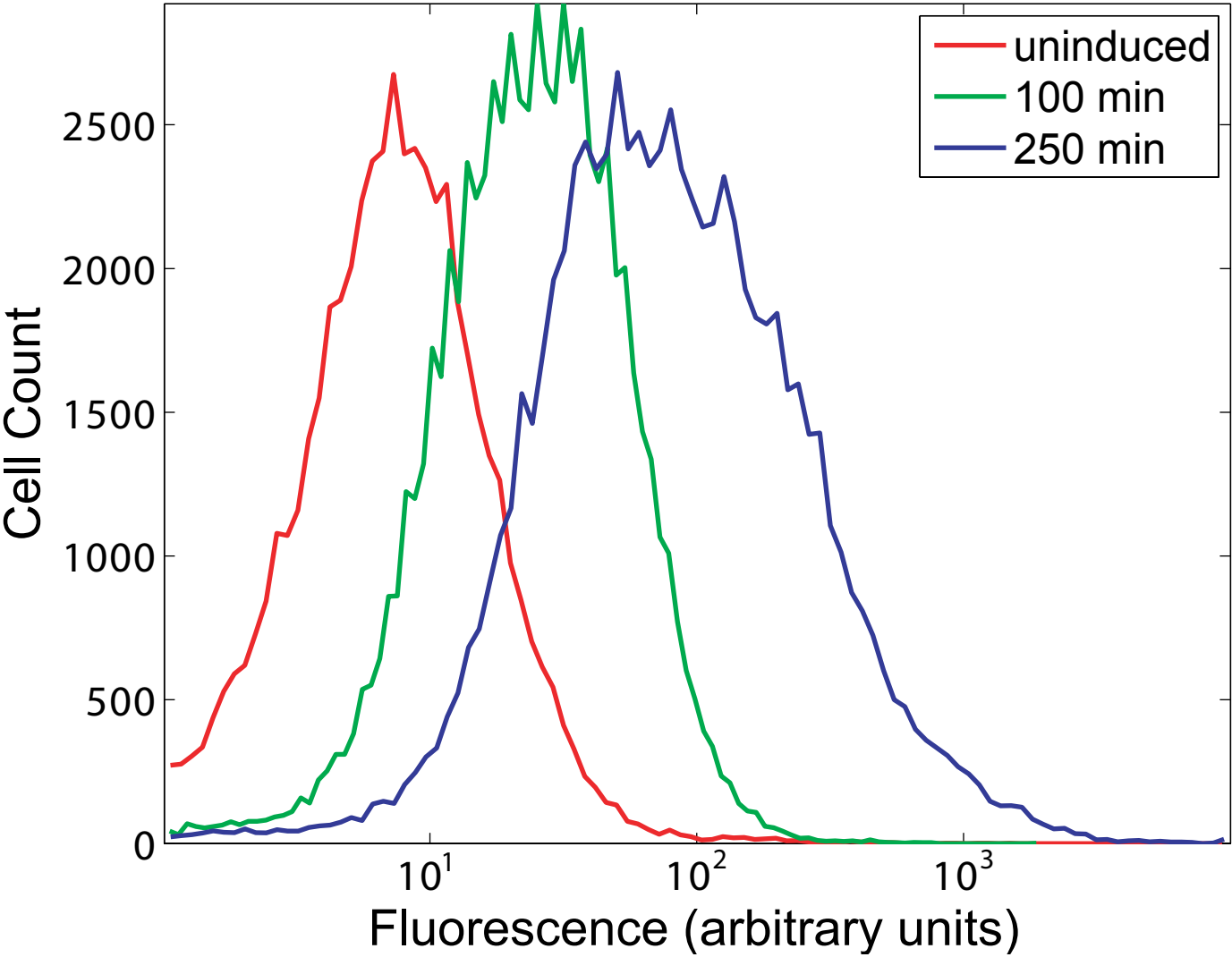
Figure S5
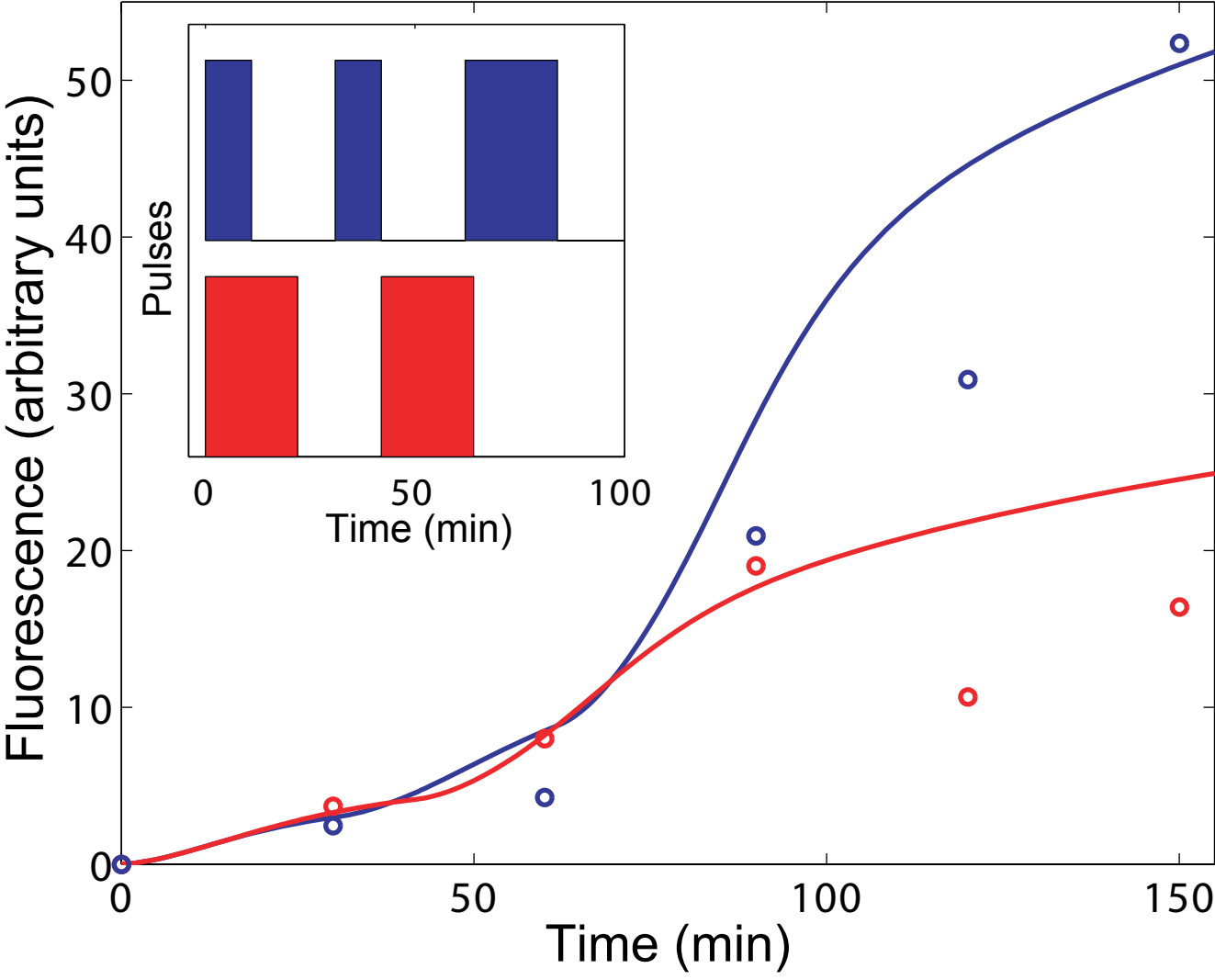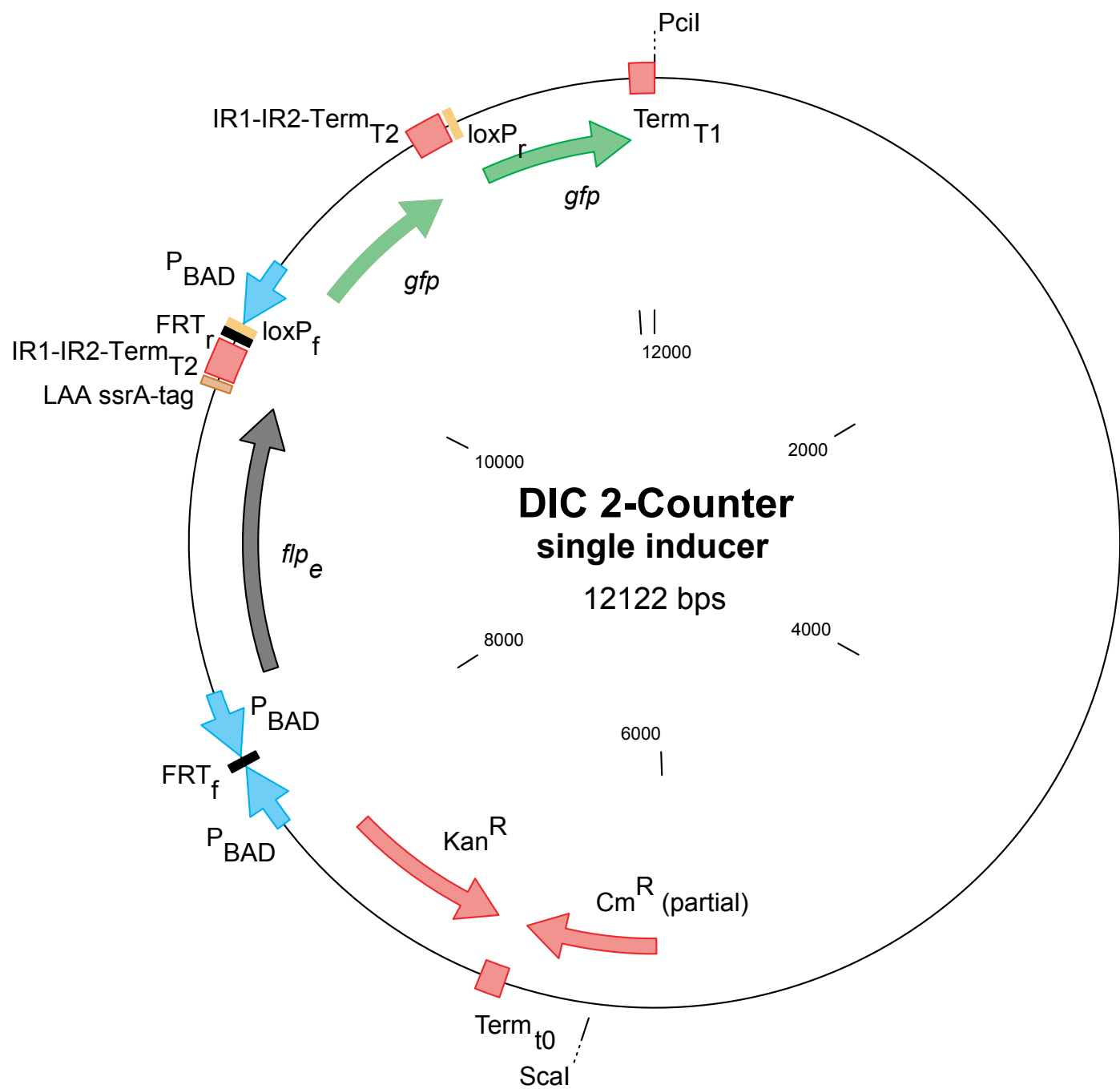
Figure S6
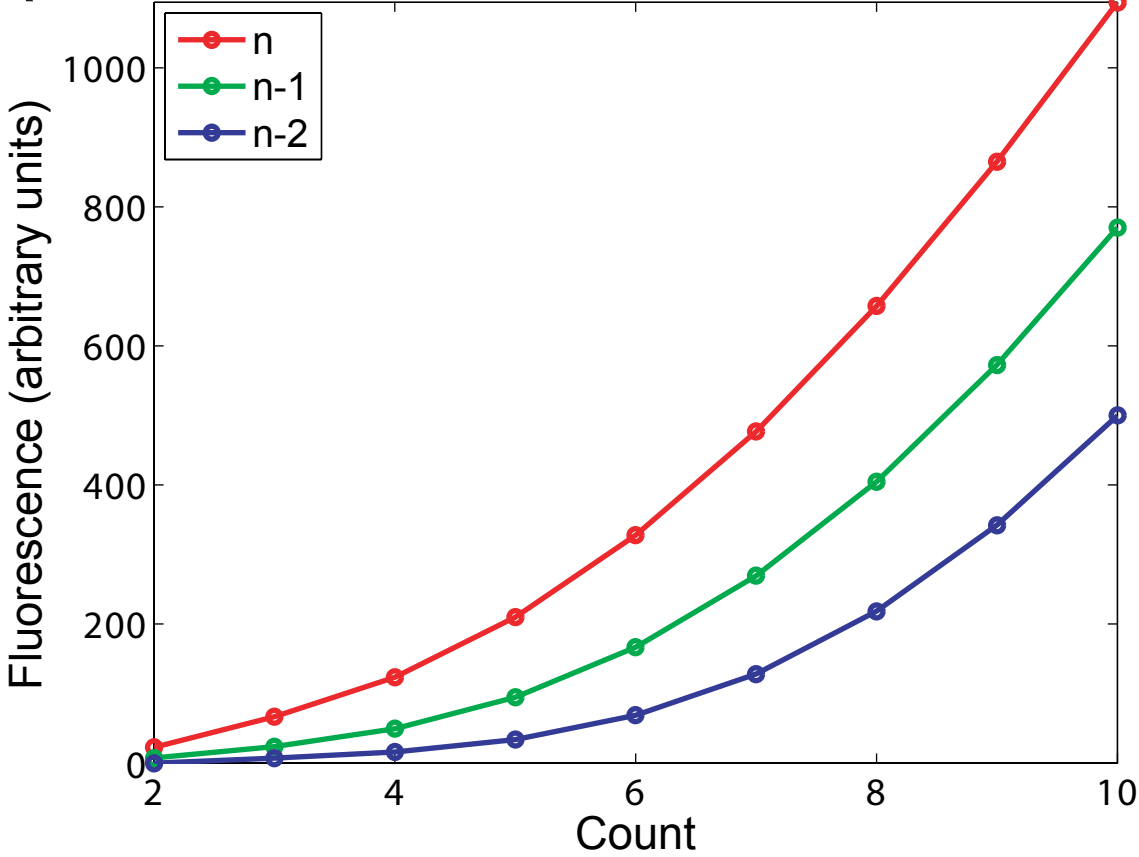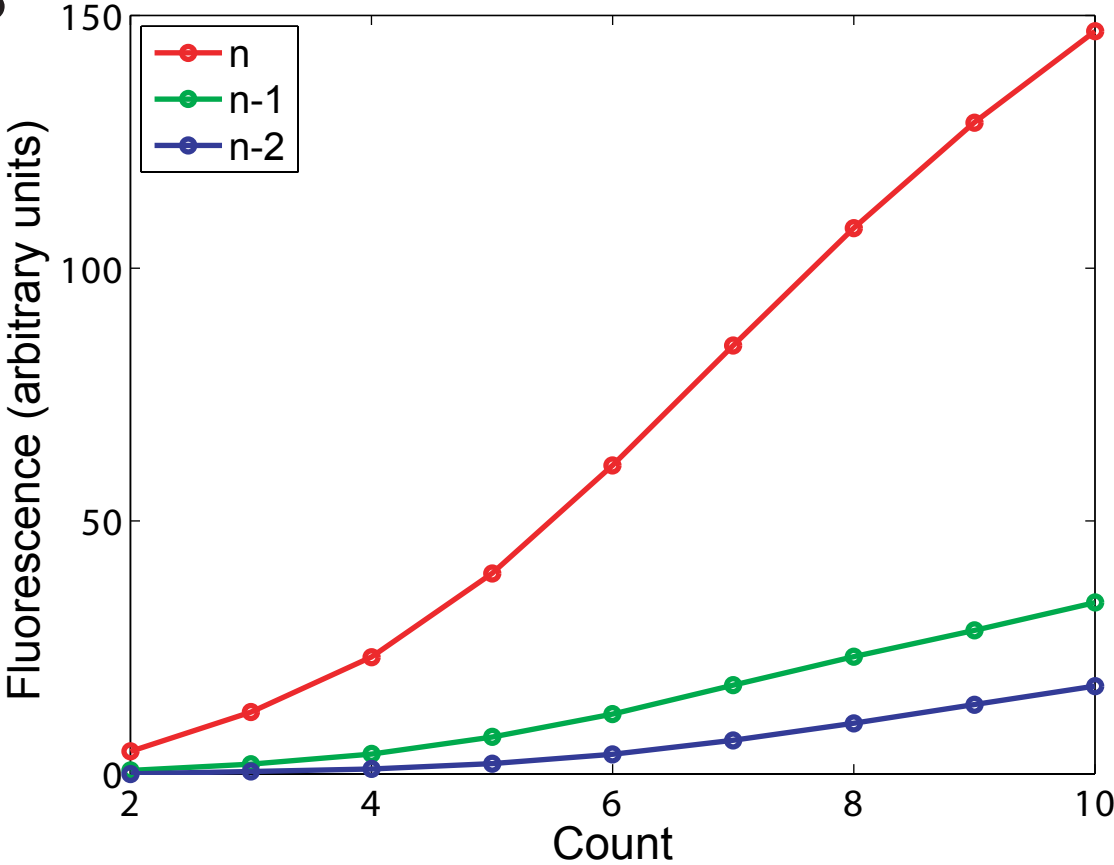
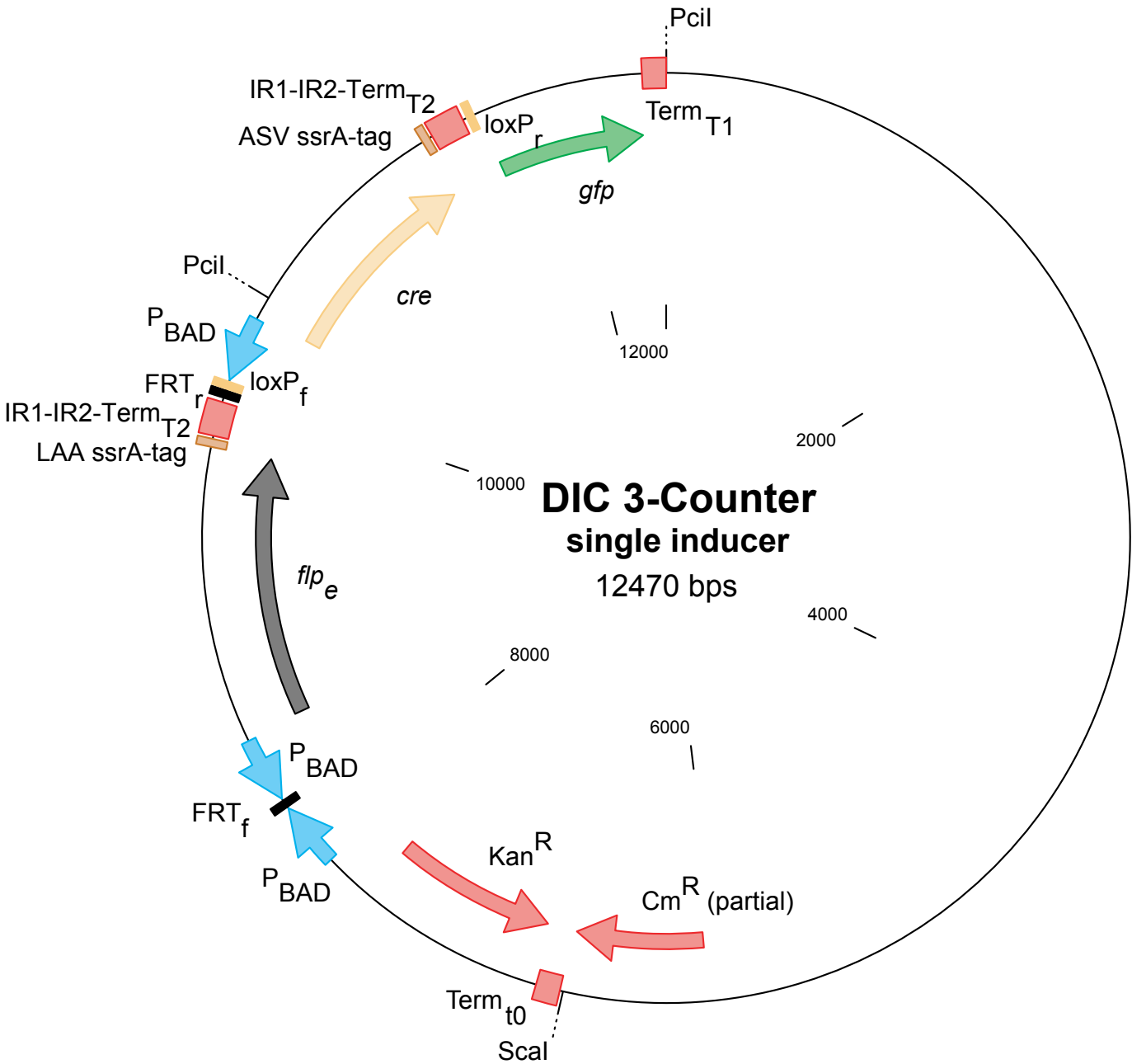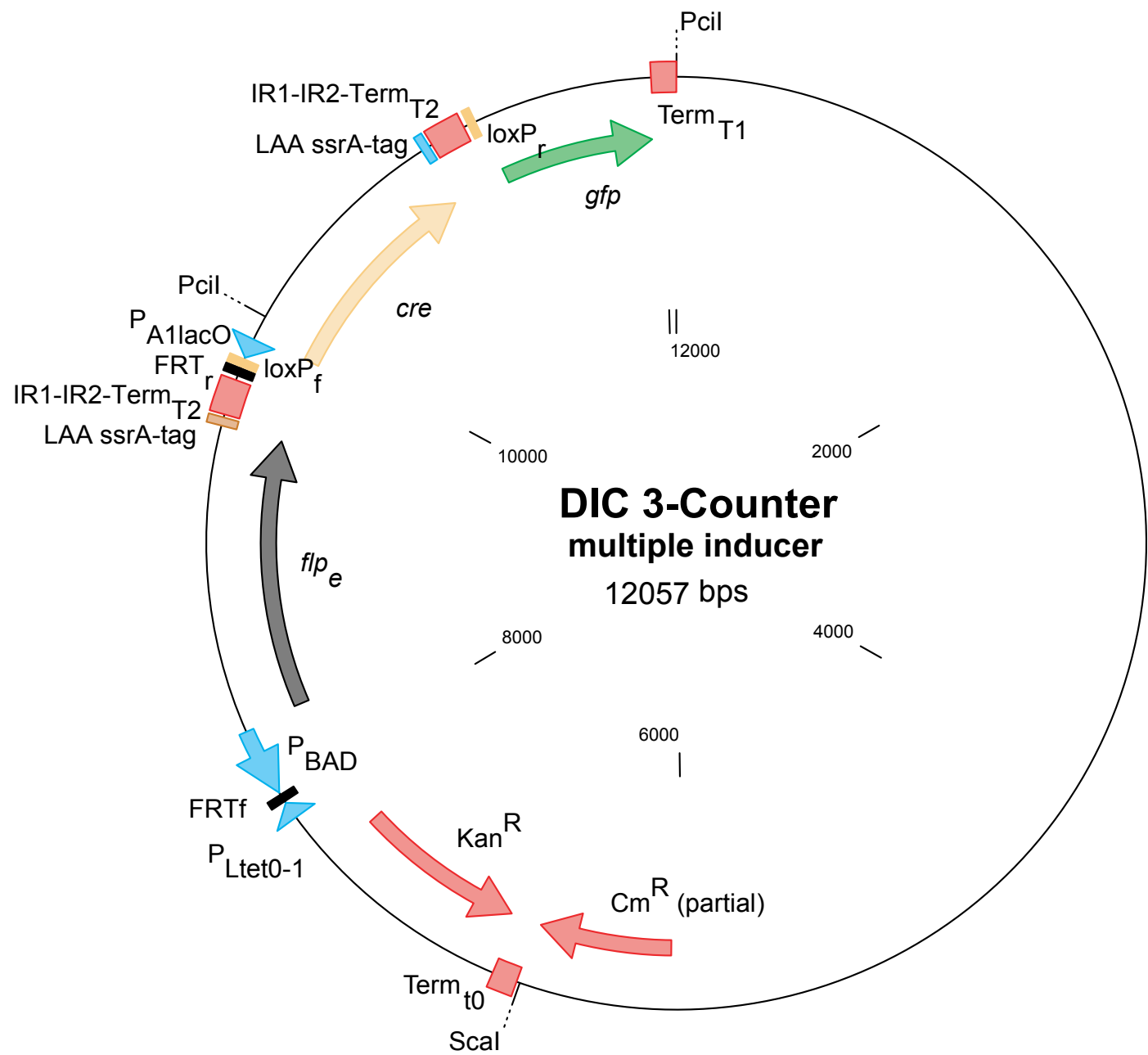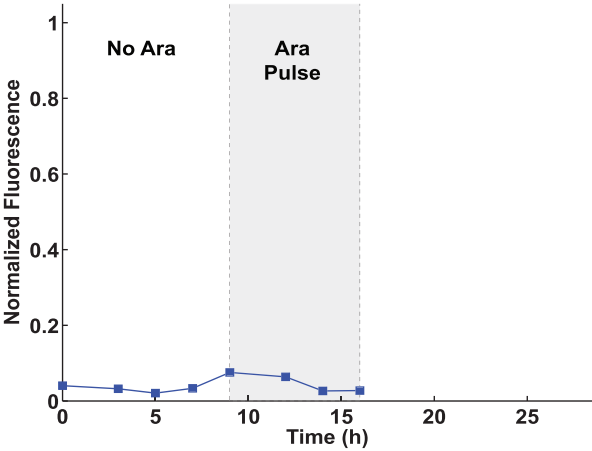# Single Invertase Memory Module (SIMM)

Figure S8

Figure S9

Plasmid map: **DIC 3-Counter single inducer** 12470 bps

Labels around the map:
- PciI
- Term$_{T1}$
- *gfp*
- loxP$_r$
- IR1-IR2-Term$_{T2}$
- ASV ssrA-tag
- *cre*
- PciI
- P$_{BAD}$
- FRT$_r$
- loxP$_f$
- IR1-IR2-Term$_{T2}$
- LAA ssrA-tag
- *flp$_e$*
- P$_{BAD}$
- FRT$_f$
- P$_{BAD}$
- Kan^R
- Cm^R (partial)
- Term$_{t0}$
- ScaI
- 2000
- 4000
- 6000
- 8000
- 10000
- 12000

Figure S10

Figure S11

A

Single Invertase Memory Module (SIMM)

B

C

Figure S12

Figure S13